 doi:10.20944/preprints202012.0641.v1

Technical Note

Rapid Immunohistological Measurement of Tyrosine Hydroxylase in Rat Midbrain by Near-Infrared Instrument-Based Detection

James W. H. Sonne [1,2,*], Corey Seavey [1,2] and Jason S. Groshong [1,2,*]

[1] Equal contributors
[2] College of Health Professions and Sciences, University of Central Florida, Orlando, FL
* Correspondence JSG: jasonsgroshong@gmail.com; Tel.: +01-(612)-598-8817 (M.N.)
* Correspondence JWHS: james.sonne@ucf.edu; Tel.: +01-(407)-823-4026 (F.L.)

Abstract: We present a robust, fresh-frozen approach to immunohistochemistry (IHC), without committing the tissue to IHC via fixation and cryopreservation while maintaining long-term storage, using LiCor-based infrared (IR) quantification for sensitive assessment of TH in immunoreacted midbrain sections for quantitative comparison across studies. In fresh-frozen tissue stored up to 1 year prior to IHC reaction, we found our method to be highly sensitive to rotenone treatment in 3-month-old Sprague-Dawley rats, and correlated with a significant decline in rotarod latency-to-fall measurement by approximately 2.5 fold. The measured midbrain region revealed a 31% lower TH signal when compared to control ($p<0.01$ by t test, $n=5$). Bivariate analysis of integrated TH counts versus rotarod latency-to-fall indicates a positive slope and modest but significant correlation of $R^2=0.68$ ($p<0.05$, $n=10$). These results indicate this rapid, instrument-based quantification method by IR detection successfully quantifies TH levels in rat brain tissue, while taking only 5 days from euthanasia to data output. This approach also allows for the identification of multiple targets by IHC with the simultaneous performance of downstream molecular analysis within the same animal tissue, allowing for the use of fewer animals per study.

Keywords: neurodegeneration; dopamine; L-DOPA; dopaminergic; DBA; Western; IR; TH; Parkinson disease

1. Introduction

Rotenone is a mitochondrial complex I inhibitor which produces systemic inflammation [1], alpha-synuclein deposition [2], microglial activation [3] and loss of motor coordination and tyrosine hydroxylase (TH) positive neurons [4] in the substantia nigra (SN), recapitulating human Parkinson's disease [5-7] much like other models [8-13]. However, rotenone develops a robust PD phenotype [14-17]. Rotenone has disadvantages in handling and storage because of its toxicity and chemical instability thus it has a short shelf life [18].

Dopamine (DA) production is rate-limited by tyrosine hydroxylase (TH) [19]. Dopaminergic neurons of the SN are tonic and their function is dependent upon the postsynaptic receptor [20-24]. The high biosynthetic activity and mitochondrial dependence of DA production lends itself to rotenone sensitivity [25-29], while dysfunction leads to the motor deficits of PD [30-32]. The rotarod instrument is used to measure motor coordination in laboratory animals and correlates with TH loss [33-35].

Our aim was to study a rodent model of parkinsonian using a sensitive and automated quantification method. The method presented here is robust because of the nature of IR detection, having a wide linear range, and is fast and impartial due to the data collection being performed by an instrument [36].

 doi:10.20944/preprints202012.0641.v1

2. Materials and Methods

The procedure presented here avoids dedicating the entire rat brain tissue to immunohistochemical analysis, allowing for multiple biochemical quantifications to be performed in the same animal. This procedure also reduces the time required to preserve and prepare the rat brain tissue prior to immunohistochemical analysis by avoiding immersion fixation and sucrose cryopreservation prior to sectioning.

Rats were randomly assigned to groups of Untreated, Vehicle-treated, and Rotenone-treated followed by pre-screening of their performance on a rotarod machine at a constant 5 rpm, as some could not be trained to perform on the rotarod, either escaping or failing to properly negotiate the rotarod. Outlier performers on rotarod were excluded from the study.

Using the Rotarod (Harvard Apparatus, LE-8305, Holliston, MA), animals were assessed for motor coordination at day 14 using the Stanford Behavioral and Functional Neuroscience Rotarod Protocol Version 4.0 [33-35]. Animals were acclimated to rotarod for 60 second monitoring at constant 5 rpm. Using the Stanford protocol to quantify motor coordination, animals were placed on rotarod at an initial 4 rpm with a constant acceleration over 300 seconds until reaching maximal 40 rpm. Latency to fall and speed at fall (rpm) were recorded for each animal. The rotarod apparatus was cleaned after each animal trial and the procedure was repeated for each animal three to five times with at least 15 minutes between each trial.

Rotenone as prepared for injection in this procedure has a shelf life of less than one week. To minimize waste while ensuring reactivity, we chose to prepare stock solutions of rotenone every 3 days. Rotenone was prepared every 3 days as a 50X stock diluted in 100% dimethyl sulfoxide DMSO (Sigma, D8418-100mL, St Louis, MO) then diluted to a final concentration of 2.8 mg/mL in 10 mL injection solution every 2 days using 100% medium chain triglyceride solution Miglyol-812N. The solutions were ensured sterile by filtration with a 0.22 μm filter (Millex, PRO3691, Cork, Ireland) and 10 cc syringe (BD, 309604, Franklin Lanes, NJ) to create the final injection solution in sterile 4 mL amber autosampler vials.

Daily intraperiotoneal injections were then performed for 14 consecutive days. Untreated animals were not injected throughout the experiment. With a ½ mL syringe (Becton Dickinson BD, 305620, Franklin Lanes, NJ), the vehicle-treated group was injected with 2% DMSO in Miglyol-812N and the rotenone group was injected with a dose of 2.8 mg/kg (1 mL/kg) rotenone in 2% DMSO in Miglyol-812N solution daily intraperitoneally (IP lower right quadrant) for 14 consecutive days.

The morning after the 14th day of treatment, animals were placed under deep anesthesia with 5% isoflurane using isoflurane vaporizer (Vet Equip, VE0615, Livermore, CA) with O2 generator (Pureline, 12219508, Clackamas, OR) scavenged on activated charcoal (Vet Equip, 931401, Livermore, CA), and followed by decapitation by guillotine. Brains were removed and prepared for sectioning followed by both immunohistochemistry and Western blotting procedures. For our Western blotting procedures, alpha-tubulin (Sigma, St. Louis, MO, USA; T9026) was used as a loading control.

All animal procedures described in this study were approved by the University of Central Florida, Institutional Animal Care and Use Committee (IACUC, A4135-01) accredited by Assessment and Accreditation of Laboratory Animal Care (AAALAC). Male, 3-month-old CD Sprague-Dawley rats (Charles River Laboratory, Catalog #24100534) were housed at room temperature (20 ± 2°C) under 12-hr light and dark cycles. The initial pilot study contained 2 animals per group as described. no differences in the untreated and vehicle groups were observed, thus they were pooled as the control group (CT). A second experiment added one more untreated animal to the CT group, and 3 more animals to the RO group, thus 5 animals for CT and 5 animals for RO, for a total of 10 animals used for the study.

Waste rotenone, animal bedding and feces, and rotenone treated animal carcasses were disposed of according to the University of Central Florida, Environmental Health

 doi:10.20944/preprints202012.0641.v1

and Safety Guidelines due to rotenone toxicity. Chemicals not specifically stated were at least molecular biology grade and purchased from Sigma (St Louis, MO).

Statistical comparisons were performed using SPSS version 25 (64-bit edition) (IBM, Armonk, NY, USA). Unless otherwise noted, one-tailed unpaired Student's t tests were performed to determine statistical significance between the CT and RO groups, defined by a p-value < 0.05.

2.1. Materials

- Rotenone (Sigma, St. Louis, MO, USA; R8875)
- 100% dimethyl sulfoxide DMSO (Sigma, St. Louis, MO, US; D8418-100mL)
- 100% medium chain triglyceride solution Miglyol-812N (IOI Oleochemicals, Hamburg, DE)
- Buffered-Formalde-Fresh (Fisher Chemical, Fair Lawn, NJ, USA; SF93-4)
- TBS:
    - 137mM NaCl (Sigma, St Louis, MO, USA; S7653-1kg)
    - 20 mM Trizma-base (Sigma, St Louis, MO, USA; T1503-500G)
    - Adjusted to a pH of 7.6 with HCl (Sigma, St Louis, MO, USA; 320331-500mL)
- 10 mM trisodium citrate (Fisher Scientific, Fair Lawn, NJ, USA; S279-500)
- 0.05% Tween-20 (Sigma, St Louis, MO, USA; P9416-50mL)
- 0.1% Triton X-100 (Sigma, St Louis, MO, USA; T8787-50mL)
- Odyssey Block Buffer TBS-based OBB (LiCor, Lincoln, NE, USA; 927-50000)
- Mouse monoclonal anti-Tyrosine Hydroxylase (Sigma St. Louis, MO, USA; MAB318)
- Goat anti-Mouse antibody-800nm (LiCor, Lincoln, NE, USA; 925-32210)
- Alpha-tubulin (Sigma, St. Louis, MO, USA; T9026)
- Hank's Balanced Salt Solution (ThermoFisher Scientific, Waltham, MA, USA; 14025126)
- OCT (Thermofisher Scientific, Waltham, MA, USA; 23-730-571)
- Isopentane (Thermofisher Scientific, Waltham, MA, USA; 02-002-082)
- cOmplete Protease Inhibitor Cocktail (Sigma, St. Louis, MO, USA; 11836153001)
- Pierce Phosphatase Inhibitor Cocktail (ThermoFisher, Waltham, MA, USA; A32957)
- Pierce Rapid Gold Assay (ThermoFisher, Waltham, MA, USA; A53225)
- 7.5 % TGX gel (BioRAD, Hercules, CA, USA; 456-1023)

2.2. Equipment

- 0.22 μm filter (Millex, Cork, Ireland; PRO3691)
- 10 cc syringe (BD, Franklin Lanes, NJ; 309604)
- ½ mL syringe (Becton Dickinson BD, 305620, Franklin Lanes, NJ)
- Rotarod (Harvard Apparatus, Holliston, MA, USA; LE-8305)
- Odyssey imaging system (LI-COR Biosciences, Model 9120, Lincoln, NE, USA)
    - Li-Cor Odyssey software (Ver. 2.1.15)
- Superfrost +/plus slides (ThermoFisher Scientific, Pittsburg, PA, USA; 12-550-15)
- Drierite dessicant without indicator (Fisher Scientific, Fair Lawn, NJ, USA; 7778-18-9)
- Super PAP Pen (Biocare Medical, Pacheco, CA, USA; PEN1111)
- Isoflurane vaporizer (Vet Equip, Livermore, CA, USA; VE0615)
- O2 generator (Pureline, Clackamas, OR, USA; 12219508)
- Activated charcoal (Vet Equip, Livermore, CA, USA; 931401)
- 1 mm (Stoelting Co, Wood Dale, IL, USA; 51388) 3. Procedure

2.3.1. Prepare Solutions. Time for Completion: 30 Minutes

1. Prepare a Homogenization Buffer in 10 mL of distilled water:
    a. 20 mM Tris Ph8
    b. 150 mM NaCl
    c. 2 mM EDTA

 doi:10.20944/preprints202012.0641.v1

d. 1% SDS
e. 1 tab cOmplete Protease Inhibitor Cocktail (Sigma, St. Louis, MO, USA; 11836153001)
f. 1 tab Pierce Phosphatase Inhibitor Cocktail (ThermoFisher, Waltham, MA, USA; A32957

2. Prepare a stock solution of20 mM Trizma-base TBS solution, pH 7.6 in 1 L distilled water:
    a. 137 mM NaCl
    b. 20 mM Trizma-base
    c. Adjust to a pH of 7.6 with HCl

2.3.2. Euthanasia & Brain Dissection. Time for Completion: 30 Minutes

3. Perform euthanasia using 5% isoflurane overdose and decapitation by guillotine.
4. Open the skull by inserting the tips of the Adson 2/1 forceps into the foramen magnum and removing the parietal bones laterally.
5. Cut the cranial nerves on the ventral side of the brain.
6. Place the brain in 4°C child Hank's Balanced Salt Solution for washing.
7. Place the brain supine in a pre-cooled 4°C stainless steel brain coronal matrix mold with slots separated at 1 mm intervals to normalize brain slices with razor blades.
8. Locate the cerebral peduncles in the ventral view and take a 2 mm section beginning at their anterior extent (corresponding approximately to Bregma -5.2 to -5.6 mm).
9. ⚠ **CRITICAL STEP** Remove the SN of the right hemisphere for Western blotting (refer to "3.3. Tissue Preparations for Western Immunoblot" below) and place in 200 µL ice cold homogenization buffer (refer to "3.1. Prepare Solutions" above).
10. Prepare to section the remaining brain tissue by placing it on cork, covering with OCT (Thermofisher Scientific, Waltham, MA, USA; 23-730-571), snap-freezing in isopentane (Thermofisher Scientific, Waltham, MA, USA; 02-002-082), then store it at -80°C until use (refer to section "3.5. Brain Tissue Sectioning" below).

2.3.2. Tissue Preparation for Western Immunoblot. Time for Completion: 45 Minutes

11. Homogenize the tissue removed SN from section "3.2" with 20 strokes in a frosted glass Tenbroek tissue grinder until visibly homogeneous.
12. Centrifuge the homogenate to remove cellular debris.
13. Quantify crude protein homogenates for equal loading using Pierce Rapid Gold Assay (ThermoFisher A53225, Waltham, MA) following the manufacturer's instructions.
14. Resolve 8 µg of homogenate on a 7.5 % TGX gel (BioRAD, 456-1023), transfer to PVDF (polyvinylidene fluoride), and immunoblotted (as described in section "3.4. Western Immunoblot").

2.3.4. Western Immunoblot. Time for Completion: 6:00 Hours

15. Block the membrane by incubating in Odyssey Block Buffer TBS-based OBB (LiCor, Lincoln, NE, USA; 927-50000) for 1 hour at room temperature (approximately 25°C)
16. Incubate with 1:1000 mouse monoclonal anti-Tyrosine Hydroxylase antibody (Sigma, St. Louis, MO, USA; MAB318) in 1:1 TBS:OBB-TBS for 1 hour at room temperature.
17. Wash three times in TBS with gentle agitation on a rocker for 10 minutes each at room temperature.
18. Incubate with 1:4000 Li-Cor goat anti-mouse antibody-800nm (LiCor, Lincoln, NE, USA; 925-32210) in 3:1 TBS:OBB-TBS for 3 hours at room temperature with gentle agitation on a rocker.
19. Wash three times in TBS with gentle agitation on a rocker for 10 minutes each at room temperature.
20. Image the membrane using an Odyssey imaging system (LI-COR Biosciences, Lincoln, NE, USA; Model 9120).

2.3.5. Brain Tissue Sectioning. Time for Completion: 1:00 Hours per brain, depending on regions of interest.

21. Remove the brain tissue from storage at -80°C and store in dry ice prior to sectioning.
22. Section on cryostat at 20 µm at -15°C and place on Superfrost +/plus slides.
    a. **OPTIONAL STEP** Place sections from four separate animals on the same slide for direct comparison.
    b. ⚠ **CRITICAL STEP** A solvent barrier is required around the border of the slides in the staining section ("3.6. TH Immunohistological Staining" below), so be careful not to place tissue sections close to the edge.

 doi:10.20944/preprints202012.0641.v1

23. Store slides in a sealed container with Drierite dessicant in a -80°C freezer until Immunohistochemical Staining (refer to section "3.6. TH Immunohistological Staining").

2.3.6. TH Immunohistological Staining. Time for Completion: 3 Days

24. Remove slides from -80°C storage and, prior to opening the sealed desiccant container, allow the container to equilibrate to room temperature (for approximately 2 hours).
25. Create a solvent barrier on the edge of the slide using a Super PAP Pen (Biocare Medical, Pacheco, CA, USA; PEN1111).
    a. ⚠ **CRITICAL STEP** If tissue is too close to the edge of the slide, trim it by scraping it away with a razor prior to this step.
26. Incubate slides for 1 minute at room temperature with Buffered-Formalde-Fresh (Fisher Chemical, Fair Lawn, NJ, USA; SF93-4)
27. Wash for 30 seconds in TBS.
28. Perform antigen retrieval overnight at 4°C in 10 mM trisodium citrate (Fisher Scientific, Fair Lawn, NJ, USA; S279-500) with 0.05% Tween-20 (Sigma, St. Louis, MO, USA; P9416-50mL) adjusted to a pH of 6 with HCl.
29. Wash 3 times for 20 minutes each in TBS with 0.1% Triton X-100 (Sigma, St. Louis, MO, USA; T8787-50mL)
30. Wash for 20 minutes with TBS.
31. Incubate for 1 hour at room temperature with Odyssey Block Buffer TBS OBB (LiCor, Lincoln, NE, USA; 927-50000).
32. Wash for 20 minutes with TBS.
33. Incubate overnight at 4°C in a humidity chamber with the primary anti-tyrosine hydroxylase monoclonal antibody (EMD Millipore, Burlington, MA, USA; MAB318) at 1:1000 in 1:1 OBB:TBS.
34. On the next day, wash 3 times for 20 minutes each in TBS.
35. Incubate for 3 hours at room temperature in a humidity chamber with the secondary antibody (Goat anti-Mouse antibody-800nm, LiCor, Lincoln, NE, USA; 925-32210) at 1:4000 dilution in 3:1 TBS:OBB.
36. Wash 3 times for 20 minutes each in TBS.
37. Wash in sterile-filtered tap water for 5 minutes.
38. Dry tissue for 1 hour prior to imaging (see section "3.7. Imaging and Quantitation" below).

2.3.7. Imaging and Quantitation. Time for Completion: 45 Minutes

39. Place slides in Li-Cor Odyssey scanner and perform quantification according to manufacturer's instructions.
40. Use a resolution of 21 μm at the highest quality with an offset of 1 mm from the scanner surface and an intensity setting of five. Excite the tissue fluorescence at 685 nm and 785 nm, and detect signal at 800 nm.
41. Trace the SN (and/or ventral tegmental area, VTA) as the region of interest (ROI) using free-hand tracing and quantitate the signal after scanning.
    a. ⚠ **CRITICAL STEP** Copy free-hand tracing ROI to unstained tissue to subtract background within the software.
    b. Choose sections for quantification by visualization of the oculomotor nerve root between the SN and VTA +/- 200 μm, corresponding approximately to Bregma -5.2, -5.4, and -5.6 mm anterior-posterior.
42. Measure multiple sections per animal and report as averages or data based on a specific anterior-posterior offset from Bregma according to your protocol.
43. **OPTIONAL STEP** Store slides at 4°C for re-imaging as needed. In our hands, sections minimal signal decay up to 1 year in storage under these conditions.

3. Results

Motor coordination assessment by rotarod is illustrated in Figure 1. Latency-to-fall measurements indicate rotenone treatment (RO) results in a 2.5 fold lower rotarod performance when compared with control (CT). (61.0 ± 8.2 vs. 173 ± 15 seconds, *$p<0.01$, n=5, mean ± SEM). No significant differences were found in untreated vs. vehicle-treated rats, (data not shown) thus they were pooled as CT.

 doi:10.20944/preprints202012.0641.v1

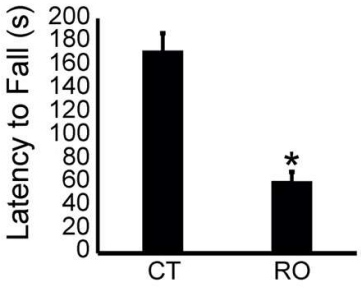

Figure 1. Motor assessment by rotarod. Latency-to-fall indicates a 2.5 fold lower rotarod performance (RO) compared with control (CT). (61.0 ± 8.2 vs. 173 ± 15 *p<0.01, n=5, mean ± SEM)

Rotenone treatment suggests a loss of tyrosine hydroxylase (TH) in the midbrain as shown (Figure 2). Homogenates of the SN were assessed by TH immunoblot suggesting a loss of TH in rotenone-treated animals (RO) when compared with control (CT), (representative data, Figure 2B) (CT = 564333±117282, RO = 140500±26600, (mean±SE), p = 0.0360 by one-tailed t test, n=3 right-hemispheres/group). The resultant quantification of TH-immunosignal in the midbrain indicates lower TH signal in the midbrain of RO animals when compared with CTs (representative images, 3 animals per group, Figure 2C). Antibody specificity is suggested by human recombinant TH block (TH Block) and reactivity with secondary antibody alone (2°) (Figure 2C). The region of interest (ROI, yellow, upper panel of Figure 2C) defined the area of measurement for IR signal (Figure 2D) performed at a digital magnification of 1.5x. Numerical counts of the TH IR signal indicate 31% lower TH signal in RO animals when compared to controls (3.32 ± 0.13 vs. 4.78 ± 0.34 x 10^6, *p<0.01, n=5, Figure 2E; scale bars = 2 mm).

 doi:10.20944/preprints202012.0641.v1

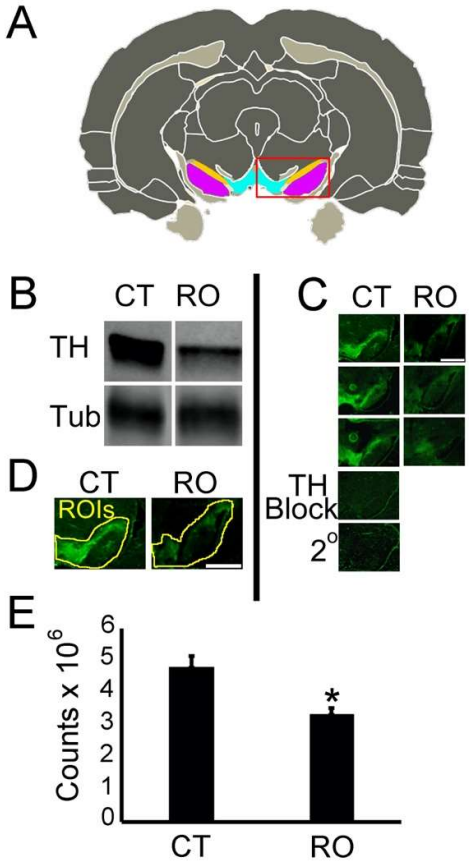

Figure 2. Rotenone treatment correlates with loss of TH detection in the midbrain. (A) Schematic of regions studied: substantia nigra pars compacta (SNpc, gold), SN pars reticulata (SNpr, magenta), and ventral tegmental area (VTA, blue, adapted from [37]). (B) SN homogenates assessed by TH immunoblot suggests a loss of TH with rotenone treatment (RO) when compared with control (CT), (representative data). (C) TH immunoreactivity in midbrain and quantification indicates a loss in TH signal primarily in the midbrain of RO animals (representative images, 3 animals per group). Antibody specificity confirmed by human recombinant TH block and 2° antibody staining alone. (D) 1.5x digital magnification of the upper panel in (C) defines the ROI (yellow) for the measurement of IR signals. (E) TH IR signal quantification indicates 31% lower TH signal in RO animals compared to controls (3.32 ± 0.13 vs. 4.78 ± 0.34 x 106, *p<0.01, n=5). Scale bars = 2mm.

Bivariate analysis of TH IR 800nm signal was performed against rotarod latency-to-fall (Figure 3). Linear regression analysis of the data set yields a slope of 12120 and y-intercept of 3 x 10^6 indicating a modestly positive, significant correlation of the data set with the estimated regression line (R^2 = 0.68, F=15.5, p<0.05, by two-way ANOVA, n=10).

Preprints (www.preprints.org) | NOT PEER-REVIEWED | Posted: 25 December 2020 doi:10.20944/preprints202012.0641.v1

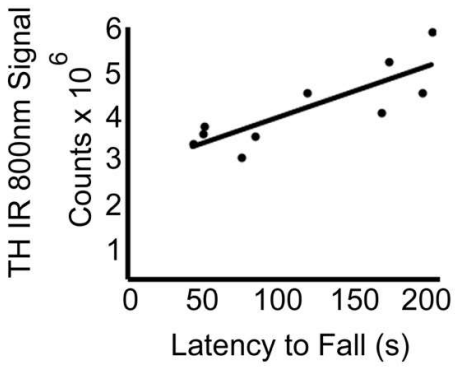

Figure 3. Bivariate analysis of TH IR 800 nm signal against motor coordination measurement by rotarod latency to fall. Linear regression analysis of the data set, yields the equation y=12120x+(3 x 10^6), indicating a positive slope, a modest correlation of the data set with the estimated regression line, and 2-way ANOVA analysis indicates the relationship is significant (R^2 = 0.68, F=15.5, p<0.05, n=10)

4. Discussion

Several reports have quantified relative tyrosine hydroxylase levels using near-infrared detection as part of a larger study [38-42]. However, the lesions were all produced differently from this report. The most common inducer was 6-OHDA injected directly into a region of the nigrostriatal pathway [38-40]. One study employed rAAV overexpression of α-synuclein [42] and another report performed a functional block/agonist approach of the histamine H1 receptor [41]. While we provide functional correlation between motor coordination and TH levels, these studies did not report correlative data on physiological or functional outcomes with TH levels. Here, we describe, for the first time, IR detection of the quantity of TH after rotenone induction.

Many important differences between our approach and previous studies involve how the brain tissue is processed. The studies cited above applied near-IR detection to traditional pre-processing involving transcardial perfusion fixation followed by a long step of immersion fixation (taking up to 7 days [40]). Fixation is followed by cryopreservation in sucrose (for a period of days, often reported as complete when the specimen sinks) prior to producing thick (40-50 uM) free-floating sections for staining [38,42]. These steps commit the tissue to histological visualization only, precluding homogenization and molecular approaches. The method we report here accomplishes the same task without fixation, making it distinct in the efficiency and flexibility it provides. In fewer steps, we present in this study an additional tool to assess TH in a method resulting in less time to complete experiments and without concerns of error or subjectivityfrom intra- and inter-observer variability. Notably, the method presented here using near-IR detection is distinct from other sources because the processing prior to staining is fast and flexible. Furthermore, valuable tissue is saved using 20 μm sections as opposed to thicker sections required by the free-floating section approach. Also, we did not perform transcardial perfusion fixation, allowing us to pursue further molecular studies as demonstrated by the TH Western blot (Figure 2B) performed on the same animal in which we performed immunohistochemical analysis, providing verification of the potential for two different methods from the same animal as a proof-of-concept. However, the gross anatomical dissection we performed for Western blot analysis is not equivalent to the precise ROI-tracing possible in the LiCor quantification. Because of the gross nature of this dissection for Western, please note that these results are not directly comparable. Western was intended merely as a validation of the potential for analysis of multiple endpoints through different methodologies in the same animal.

Our present method circumvents the weeks of post-processing by using our fresh frozen approach, where the specimen remains frozen continuously until the section contacts the slide at room temperature, at which time it desiccates within about 20-30 seconds. This rapid desiccation serves some of the same purposes as the traditional sucrose-mediated cryopreservation step. During long-term storage at -80°C, we found that we could still detect robust differences in TH levels when comparing RO to CT up to 1 year after harvest from tissue blocks and 6-9 months from fresh frozen mounted slides. The data from tissue treated in this manner indicate that our method sufficiently preserves the specimens to detect differences in TH signal.

We have presented near-IR detection of TH derived from a gross, anatomy-traced format, which may be considered a limitation of the method. Our quantitation included the anatomically adjacent ventral tegmental area, but researchers may choose to limit their anatomical analysis to different regions or nuclei using the same approach. Future advances to this methodology might employ a second target for multiple outcome measures or a control protein that might provide a measure for ratiometric normalization. Conceptually comparing our method to DAB detection of TH in the SNpc and Str, near-IR detection has a greater linear range of detection compared DAB detection due to the enzymatic, exponential nature of DAB, suggesting that the presented near-IR methodology is more capable of detecting subtle changes in TH levels, such as at the early stages of cellular stress; however, future studies are needed to address which detection methods are more statistically sensitive and appropriate for specific study endpoints. Our use of the outbred Sprague-Dawley rats was intentional, as the inter-animal variability represents the variability in the human population. With our technique, we report significant differences with an n=5 per group in this out-bred rat model. Refinement of the molecular target and anatomical regions and nuclei for future studies could benefit different study aims. The effects of long-term storage and tissue handling reported here on the detection of other targets are also not quantified. We have explored the detection of other targets with some success detecting CD11b, a pan microglial marker, in these same tissues using a fluorescence detection approach (data not published). Remarkably, we have also had some success detecting microglial markers by fluorescence approaches on tissues that have already been processed for near-IR TH studies (data not published). If successful in these re-staining approaches, it will be possible to use tissue previously stained and detected by near-IR for re-staining with immunofluorescent antibodies by epifluorescence microscopy. With this advance in the technique, researchers have the capability to study a multitude of targets dependent only upon the number of near-IR and fluorescent probes available for each tissue per slide, allowing researchers to address more questions with fewer tissue sections and possibly with smaller cohorts of animals.

5. Conclusions

The methods present in the present provide an automated method of quantifying expressed TH levels in sectioned rat brain tissue. We report that the presence of TH signal correlates with motor coordination and show that immunohistochemical detection of TH enzyme by IR-linked secondary antibody may provide a useful measure. We achieve statistical significance with only 5 animals per group, indicating the statistical power of the method using a method without subjective assessment. Our data is presented as its raw output, without normalization or transformation, and so can be directly compared with other studies that use the technique. The presented fresh frozen section approach allows for multiple methodologies in the same tissue, and the time from animal euthanasia to data output can be completed in roughly 5 working days. Furthermore, the fresh frozen tissues presented in this study have been under long-term storage conditions for up to one year prior to immunoreaction and quantification. Once scanned, the saved images can be presented as raw data that can be quantified independently using reported settings to mitigate irreproducibility in reported immunohistological endpoint determination. Using this method also allowed us to reduce the number of animals used while measuring

multiple endpoints. We invite other investigators to validate our approach and to expand its use to other model systems.

Author Contributions: All authors have read and agree to the published version of the manuscript. Conceptualization, J.G. and J.S.; methodology, J.G.; validation, J.G., C.S.; formal analysis, J.G.; data curation, J.G. and C.S.; writing—original draft preparation, J.G.; writing—review and editing, J.G, C.S., and J.S..; visualization, J.G.; supervision, J.S.; project administration, J.S.; funding acquisition, J.S.

Funding: This research received no external funding. This research was funded by University of Central Florida Provost Start-up funds and the Pre-eminent Post-Doctoral Program funding for James W. H. Sonne and Jason S. Groshong.

Acknowledgments: The authors would like to acknowledge Jason R. Cannon, Ph.D. of Purdue University for many useful discussions regarding the rotenone IP injection rat model of Parkinson's disease and for providing Miglyol-812N for use in our rotenone solution. We would also like to thank our students Cullen Lemieux and Cheyanne Frosti B.S., M.S., for many useful suggestions and discussions pertaining to this study.

Conflicts of Interest: The authors declare no conflict of interest. The funders had no role in the design of the study; in the collection, analyses, or interpretation of data; in the writing of the manuscript, or in the decision to publish the results.

References

1. Liang, Y.; Zhou, T.; Chen, Y.; Lin, D.; Jing, X.; Peng, S.; Zheng, D.; Zeng, Z.; Lei, M.; Wu, X., et al. Rifampicin inhibits rotenone-induced microglial inflammation via enhancement of autophagy. Neurotoxicology 2017, 63, 137-145, doi:S0161-813X(17)30204-8 [pii] 10.1016/j.neuro.2017.09.015.
2. Zhang, Z.N.; Zhang, J.S.; Xiang, J.; Yu, Z.H.; Zhang, W.; Cai, M.; Li, X.T.; Wu, T.; Li, W.W.; Cai, D.F. Subcutaneous rotenone rat model of Parkinson's disease: Dose exploration study. Brain Res 2017, 1655, 104-113, doi:S0006-8993(16)30776-4 [pii] 10.1016/j.brainres.2016.11.020.
3. Sherer, T.B.; Betarbet, R.; Kim, J.H.; Greenamyre, J.T. Selective microglial activation in the rat rotenone model of Parkinson's disease. Neurosci Lett 2003, 341, 87-90, doi:10.1016/s0304-3940(03)00172-1.
4. Cannon, J.R.; Tapias, V.; Na, H.M.; Honick, A.S.; Drolet, R.E.; Greenamyre, J.T. A highly reproducible rotenone model of Parkinson's disease. Neurobiol Dis 2009, 34, 279-290.
5. Monahan, A.J.; Warren, M.; Carvey, P.M. Neuroinflammation and peripheral immune infiltration in Parkinson's disease: an autoimmune hypothesis. Cell Transplant 2008, 17, 363-372.
6. Betarbet, R.; Sherer, T.B.; MacKenzie, G.; Garcia-Osuna, M.; Panov, A.V.; Greenamyre, J.T. Chronic systemic pesticide exposure reproduces features of Parkinson's disease. Nat Neurosci 2000, 3, 1301-1306, doi:10.1038/81834.
7. Sherer, T.B.; Kim, J.H.; Betarbet, R.; Greenamyre, J.T. Subcutaneous rotenone exposure causes highly selective dopaminergic degeneration and alpha-synuclein aggregation. Exp Neurol 2003, 179, 9-16, doi:10.1006/exnr.2002.8072.
8. Zuddas, A.; Fascetti, F.; Corsini, G.U.; Piccardi, M.P. In brown Norway rats, MPP+ is accumulated in the nigrostriatal dopaminergic terminals but it is not neurotoxic: a model of natural resistance to MPTP toxicity. Exp Neurol 1994, 127, 54-61, doi:10.1006/exnr.1994.1079.
9. Kalinina, T.S.; Nerobkova, L.N.; Voronina, T.A.; Stovbun, S.V.; Litvin, A.A.; Sergienko, V.I. Study of antiparkinsonic activity of panavir on a model of Parkinson syndrome induced by systemic administration of MPTP to outbred rats and C57Bl/6 mice. Bull Exp Biol Med 2005, 140, 55-57, doi:10.1007/s10517-005-0410-3.
10. Cenci, M.A.; Lundblad, M. Ratings of L-DOPA-induced dyskinesia in the unilateral 6-OHDA lesion model of Parkinson's disease in rats and mice. Curr Protoc Neurosci 2007, Chapter 9, Unit 9 25, doi:10.1002/0471142301.ns0925s41.
11. Truong, L.; Allbutt, H.; Kassiou, M.; Henderson, J.M. Developing a preclinical model of Parkinson's disease: a study of behaviour in rats with graded 6-OHDA lesions. Behav Brain Res 2006, 169, 1-9, doi:10.1016/j.bbr.2005.11.026.
12. Robinson, T.E.; Becker, J.B. The rotational behavior model: asymmetry in the effects of unilateral 6-OHDA lesions of the substantia nigra in rats. Brain Res 1983, 264, 127-131, doi:10.1016/0006-8993(83)91129-0.
13. Stenslik, M.J.; Potts, L.F.; Sonne, J.W.; Cass, W.A.; Turchan-Cholewo, J.; Pomerleau, F.; Huettl, P.; Ai, Y.; Gash, D.M.; Gerhardt, G.A., et al. Methodology and effects of repeated intranasal delivery of DNSP-11 in a rat model of Parkinson's disease. J Neurosci Methods 2015, 251, 120-129, doi:10.1016/j.jneumeth.2015.05.006.
14. Johnson, M.E.; Salvatore, M.F.; Maiolo, S.A.; Bobrovskaya, L. Tyrosine hydroxylase as a sentinel for central and peripheral tissue responses in Parkinson's progression: Evidence from clinical studies and neurotoxin models. Prog Neurobiol 2018, 165-167, 1-25, doi:10.1016/j.pneurobio.2018.01.002.
15. Anderson, D.W.; Bradbury, K.A.; Schneider, J.S. Neuroprotection in Parkinson models varies with toxin administration protocol. Eur J Neurosci 2006, 24, 3174-3182, doi:10.1111/j.1460-9568.2006.05192.x.

16. Ferro, M.M.; Bellissimo, M.I.; Anselmo-Franci, J.A.; Angellucci, M.E.; Canteras, N.S.; Da Cunha, C. Comparison of bilaterally 6-OHDA- and MPTP-lesioned rats as models of the early phase of Parkinson's disease: histological, neurochemical, motor and memory alterations. J Neurosci Methods 2005, 148, 78-87, doi:10.1016/j.jneumeth.2005.04.005.
17. Schober, A. Classic toxin-induced animal models of Parkinson's disease: 6-OHDA and MPTP. Cell Tissue Res 2004, 318, 215-224, doi:10.1007/s00441-004-0938-y.
18. Bowman, M.C.; Holder, C.L.; Bone, L.I. High pressure liquid chromatographic determination of rotenone and degradation products in animal chow and tissues. J Assoc Off Anal Chem 1978, 61, 1445-1455.
19. Daubner, S.C.; Le, T.; Wang, S. Tyrosine hydroxylase and regulation of dopamine synthesis. Arch Biochem Biophys 2011, 508, 1-12, doi:10.1016/j.abb.2010.12.017.
20. Radulescu, A.R. Mechanisms explaining transitions between tonic and phasic firing in neuronal populations as predicted by a low dimensional firing rate model. PLoS One 2010, 5, e12695, doi:10.1371/journal.pone.0012695.
21. Wang, L.; Liang, P.J.; Zhang, P.M.; Qiu, Y.H. Ionic mechanisms underlying tonic and phasic firing behaviors in retinal ganglion cells: a model study. Channels (Austin) 2014, 8, 298-307, doi:10.4161/chan.28012.
22. Sonne, J.; Lopez-Ojeda, W. Dopamine. In StatPearls, Treasure Island (FL), 2019.
23. Sonne, J.; Beato, M.R. Neuroanatomy, Substantia Nigra. In StatPearls, Treasure Island (FL), 2019.
24. Swarnkar, S.; Singh, S.; Mathur, R.; Patro, I.K.; Nath, C. A study to correlate rotenone induced biochemical changes and cerebral damage in brain areas with neuromuscular coordination in rats. Toxicology 2010, 272, 17-22, doi:10.1016/j.tox.2010.03.019.
25. Lin, T.K.; Cheng, C.H.; Chen, S.D.; Liou, C.W.; Huang, C.R.; Chuang, Y.C. Mitochondrial dysfunction and oxidative stress promote apoptotic cell death in the striatum via cytochrome c/caspase-3 signaling cascade following chronic rotenone intoxication in rats. Int J Mol Sci 2012, 13, 8722-8739, doi:10.3390/ijms13078722.
26. Al-Lahham, R.; Deford, J.H.; Papaconstantinou, J. Mitochondrial-generated ROS down regulates insulin signaling via activation of the p38MAPK stress response pathway. Mol Cell Endocrinol 2016, 419, 1-11, doi:10.1016/j.mce.2015.09.013 S0303-7207(15)30079-4 [pii].
27. Berbusse, G.W.; Woods, L.C.; Vohra, B.P.; Naylor, K. Mitochondrial Dynamics Decrease Prior to Axon Degeneration Induced by Vincristine and are Partially Rescued by Overexpressed cytNmnat1. Front Cell Neurosci 2016, 10, 179, doi:10.3389/fncel.2016.00179.
28. Zhang, L.; Hao, J.; Zheng, Y.; Su, R.; Liao, Y.; Gong, X.; Liu, L.; Wang, X. Fucoidan Protects Dopaminergic Neurons by Enhancing the Mitochondrial Function in a Rotenone-induced Rat Model of Parkinson's Disease. Aging Dis 2018, 9, 590-604, doi:10.14336/AD.2017.0831.
29. Jiang, X.; Tang, P.C.; Chen, Q.; Zhang, X.; Fan, Y.Y.; Yu, B.C.; Gu, X.X.; Sun, Y.; Ge, X.Q.; Zhang, X.L. Neuroprotective effects of cordycepin with anti-apoptosis mechanism based on mitochondrial pathway in rotenone-induced parkinsonism rat model. CNS Neurol Disord Drug Targets 2019, 10.2174/1871527318666190905152138, doi:10.2174/1871527318666190905152138.
30. Kaasinen, V.; Kinos, M.; Joutsa, J.; Seppanen, M.; Noponen, T. Differences in striatal dopamine transporter density between tremor dominant and non-tremor Parkinson's disease. Eur J Nucl Med Mol Imaging 2014, 41, 1931-1937, doi:10.1007/s00259-014-2796-5.
31. Lindner, M.D.; Cain, C.K.; Plone, M.A.; Frydel, B.R.; Blaney, T.J.; Emerich, D.F.; Hoane, M.R. Incomplete nigrostriatal dopaminergic cell loss and partial reductions in striatal dopamine produce akinesia, rigidity, tremor and cognitive deficits in middle-aged rats. Behav Brain Res 1999, 102, 1-16, doi:10.1016/s0166-4328(98)00160-0.
32. Kelly, D.M.; Naylor, R.J. An intracerebral injection study on the role of striatal dopamine and 5-hydroxytryptamine in the production of tremor by harmine. Neuropharmacology 1976, 15, 303-308, doi:10.1016/0028-3908(76)90133-7.
33. Portmann, T.; Yang, M.; Mao, R.; Panagiotakos, G.; Ellegood, J.; Dolen, G.; Bader, P.L.; Grueter, B.A.; Goold, C.; Fisher, E., et al. Behavioral abnormalities and circuit defects in the basal ganglia of a mouse model of 16p11.2 deletion syndrome. Cell Rep 2014, 7, 1077-1092, doi:10.1016/j.celrep.2014.03.036 S2211-1247(14)00214-9 [pii].
34. McFadyen, M.P.; Kusek, G.; Bolivar, V.J.; Flaherty, L. Differences among eight inbred strains of mice in motor ability and motor learning on a rotorod. Genes Brain Behav 2003, 2, 214-219.
35. Faizi, M.; Bader, P.L.; Tun, C.; Encarnacion, A.; Kleschevnikov, A.; Belichenko, P.; Saw, N.; Priestley, M.; Tsien, R.W.; Mobley, W.C., et al. Comprehensive behavioral phenotyping of Ts65Dn mouse model of Down syndrome: activation of beta1-adrenergic receptor by xamoterol as a potential cognitive enhancer. Neurobiol Dis 2011, 43, 397-413, doi:10.1016/j.nbd.2011.04.011 S0969-9961(11)00128-8 [pii].
36. Shutz-Geschwender, A., Zhang, Y, Holt T, McDermitt, and Olive, M.D. Quantitative, Two-Color Western Blot Detection With Infrared Fluorescence. LI-COR Biosciences 2004, 1-8.
37. Papp, E. A., Leergaard, T. B., Calabrese, E., Johnson, G. A., Bjaalie, J. G. Waxholm Space atlas of the Sprague Dawley rat brain. Neuroimage 2014, 97:374-86.
38. Gagnon, D., Petryszyn, S., Sanchez, M.G., Bories, C., Beaulieu, J.M., De Koninck, Y., Parent, A., Parent, M. Striatal Neurons Expressing D1 and D2 Receptors are Morphologically Distinct and Differently Affected by Dopamine Denervation in Mice. Sci Rep. 2017, 7, 41432.

 doi:10.20944/preprints202012.0641.v1

39. Gombash, S.E., Manfredsson, F.P., Kemp, C.J., Kuhn, N.C., Fleming, S.M., Egan, A.E., Grant, L.M., Ciucci, M.R., MacKeigan, J.P., Sortwell, C.E. Morphological and behavioral impact of AAV2/5-mediated overexpression of human wildtype alpha-synuclein in the rat nigrostriatal system. PLoS One 2013, 8(11), e81426.
40. Gombash, S.E., Manfredsson, F.P., Mandel, R.J., Collier, T.J., Fischer, D.L., Kemp, C.J., Kuhn, N.M., Wohlgenant, S.L., Fleming, S.M., Sortwell, C.E. Neuroprotective potential of pleiotrophin overexpression in the striatonigral pathway compared with overexpression in both the striatonigral and nigrostriatal pathways. Gene Ther 2014, 21(7), 682-693.
41. Marquez-Valadez, B., Aquino-Miranda, G., Quintero-Romero, M.O., Papacostas-Quintanilla, H., Bueno-Nava, A., Lopez-Rubalcava, C., Diaz, N.F., Arias-Montano, J.A., Molina-Hernandez, A. The Systemic Administration of the Histamine H1 Receptor Antagonist/Inverse Agonist Chlorpheniramine to Pregnant Rats Impairs the Development of Nigro-Striatal Dopaminergic Neurons. Front Neurosci 2019, 13, 360.
42. Paumier, K.L., Luk, K.C., Manfredsson, F.P., Kanaan, N.M., Lipton, J.W., Collier, T.J., Steece-Collier, K., Kemp, C.J., Celano, S., Schulz, E., Sandoval, I.M., Fleming, S., Dirr, E., Polinski, N.K., Trojanowski, J.Q., Lee, V.M., Sortwell, C.E. Intrastriatal injection of pre-formed mouse alpha-synuclein fibrils into rats triggers alpha-synuclein pathology and bilateral nigrostriatal degeneration. Neurobiol Dis 2015, 82, 185-199.